






Article

A Prototype Photoplethysmography Electronic Device that Distinguishes Congestive Heart Failure from Healthy Individuals by Applying Natural Time Analysis

George Baldoumas ^{1,2}, Dimitrios Peschos ¹, Giorgos Tatsis ² , Spyridon K. Chronopoulos ^{2,*} , Vasilis Christofilakis ^{2,*} , Panos Kostarakis ², Panayiotis Varotsos ³, Nicholas V. Sarlis ³ , Efthimios S. Skordas ³ , Aris Bechlioulis ⁴, Lampros K. Michalis ⁴ and Katerina K. Naka ⁴

¹ Faculty of Medicine, University of Ioannina, 451 10 Ioannina, Greece; gbaldoumas@uoi.gr (G.B.); dpeschos@uoi.gr (D.P.)

² Electronics-Telecommunications and Applications Laboratory, Physics Department, University of Ioannina, 451 10 Ioannina, Greece; gtatsis@grads.uoi.gr (G.T.); panos.kostarakis@gmail.com (P.K.)

³ Section of Solid State Physics, Department of Physics, National and Kapodistrian University of Athens, Panepistimiopolis, 157 84 Zografos, Athens, Greece; pvaro@phys.uoa.gr (P.V.); nsarlis@phys.uoa.gr (N.V.S.); eskordas@phys.uoa.gr (E.S.S.)

⁴ Michaelidion Cardiac Center, 2nd Department of Cardiology and Michaelidion Cardiac Center, Medical School, University of Ioannina, 45110 Ioannina, Greece; md02798@yahoo.gr (A.B.); lmihalis@cc.uoi.gr (L.K.M.); anaka@cc.uoi.gr (K.K.N.)

* Correspondence: schrono@cc.uoi.gr (S.K.C.); vachrist@uoi.gr (V.C.); Tel.: +30-26510-08635 (S.K.C.); +30-26510-08542 (V.C.)

Received: 28 September 2019; Accepted: 2 November 2019; Published: 5 November 2019



Abstract: In this paper, a prototype photoplethysmography (PPG) electronic device is presented for the distinction of individuals with congestive heart failure (CHF) from the healthy (H) by applying the concept of Natural Time Analysis (NTA). Data were collected simultaneously with a conventional three-electrode electrocardiography (ECG) system and our prototype PPG electronic device from H and CHF volunteers at the 2nd Department of Cardiology, Medical School of Ioannina, Greece. Statistical analysis of the results show a clear separation of CHF from H subjects by means of NTA for both the conventional ECG system and our PPG prototype system, with a clearly better distinction for the second one which additionally inherits the advantages of a low-cost portable device.

Keywords: Natural Time; algorithm; electrocardiography; photoplethysmography; non-invasive electronic device; sensors; Pan-Tomkins algorithm; signal processing

1. Introduction

In recent decades, the technological revolution has helped the medical science in the prognosis, diagnosis, and monitoring of patients. In cardiology there has been significant progress in recording the Heart Rate Variability (HRV) which is directly related to major pathological heart conditions. Beyond the standard electrocardiogram (ECG) characterized by a sequence of P, QRS, and T waves, in recent years, a technique termed photoelectric plethysmography, also known as photoplethysmography (PPG), has simplified the recording of heart rate in an easy and reliable way [1,2]. From 1980 the PPG method has been used as pulse oximeter for monitoring a person's oxygen saturation into clinical care. Nowadays the PPG technology is included in many modern affordable devices such as smart phones, smart watches, tablets, bracelets, rings, etc. It is a simple technique with low cost and

gives us health-related information such as HRV, blood oxygen saturation (SpO_2), blood pressure, and respiratory rate [3,4].

Cardiac function is based on an electrical circuit that controls heart rate and synchronizes the operation of ventricles and atria, thereby sending effectively blood to all vital organs. The reduced ability of the heart to pump and/or fill with blood could lead to Heart Failure (HF) [5], also known as congestive heart failure (CHF). HF is a complicated syndrome affecting 1%–2% of the population in the developed world and at least 26 million people worldwide and is increasing in prevalence especially in the elderly populations [6,7]. HF is a clinical syndrome that is related to the presence of symptoms of increased fatigue and reduced functional capacity but may also lead to sudden cardiac death due to cardiac arrhythmias. Currently, the diagnosis of HF is based on clinical, echocardiographic, and biochemical markers that are evident late in the progress of HF syndrome [8]. Cardiac dysfunction associated with the presence of HF is often related to electrical cardiac abnormalities.

Several studies have attempted to find differences of the autonomic nervous cardiac system that controls the electrical cardiac function between patients with HF and healthy (H) subjects using a variety of algorithms of pattern recognition primary based on long term data [9]. Computer aided detection methods for automatic HF diagnosis using ECG signals have been reported in literature [10]. Although these methods still harbor several limitations there is evidence for increased benefit in using nonlinear features for the automated diagnosis of HF with ECG signals [10]. However, since physiological time series may be due to a mixed process, stochastic, and deterministic, the use of fractal dimensions in physiological time series has been occasionally criticized (see [11] and references therein; see also [12]).

The Natural Time Analysis (NTA) has been applied to complex dynamical systems in various scientific fields, such as Geosciences [13–16], Seismology [13,16,17], Physics [14,18,19], Biology [13,14], and Medicine [13,20–24] including applications to ECG focused on the distinction of H from Sudden Cardiac Death (SCD) individuals [20,21,23] as well as from HF individuals [20,21,24]. This distinction is based on the entropy S defined in NTA which is a dynamic entropy depending on the sequential order of pulses and fundamentally different [20,23] than other entropies reviewed in [10]. NTA plays an important role in identifying when a complex system approaches a phase change (dynamic phase transition, in which a critical point is defined). We clarify that this concept of entropy is equally applicable to deterministic as well as stochastic processes. This is the first work that employs NTA in the complex dynamical system of the heart by using data obtained by a low-cost portable accurate PPG electronic device as well as by ECG and compares the results. Furthermore, from the results it is evident that a clear distinction of H from HF individuals may be achieved through a small time window. This method may aid, even when ECG are not available, in the diagnosis of HF syndrome and the identification of HF patients at higher risk for SCD by means of portable PPG data.

2. Materials and Methods

2.1. Conventional ECG System

The first system was a portable wearable electrocardiograph with commercial name BioRadio from the Great Lakes NeuroTechnologies Company. This ECG has programmable channels for recording and transmitting combinations of human physiological signals, providing a standardized method of wireless and mobile ECG measurement. As shown in Figure 1, the ECG is connected through three high performance foam snap electrodes which contacts on the individual's skin and enables reliable connections with lead wires. The ECG system digitized the signal at 4000 samples per second, with 16 bit resolution, and transferred the data via Bluetooth connection to a laptop.

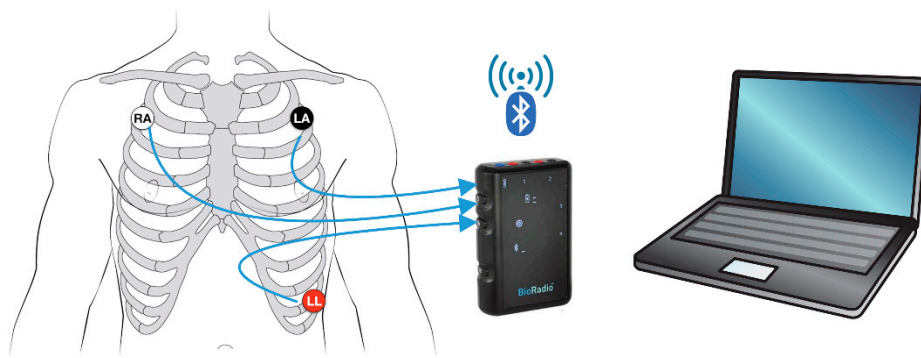


Figure 1. The conventional electrocardiogram (ECG) system.

2.2. Prototype PPG System

The second system comprises from a low-cost portable accurate PPG electronic device which measures the heart rate from the individual's finger and a host (PC, laptop, etc.) where signal processing and NTA were performed offline. This device was designed and assembled in Electronics-Telecommunications and Applications Laboratory of the Physics Department, University of Ioannina, Greece while the accuracy of the initial device, in terms of heart rate measurements, has been confirmed in [11] (where comparison of the RR intervals in ECG and oximeter signals has been made). Figure 2 shows the connection between PPG and a laptop while the prototype electronic device is shown in Figure 3. The PPG device is comprised of two parts. The first one includes a finger heart rate monitor sensor based on the MAX30100 module from Maxim Integrated Company which is using the PPG technique. It combines two LEDs (Light Emitting Diodes), one emitting red light, and another emitting infrared light. We used the infrared light since we found better PPG signal instead of the red light. Furthermore, it has a photodetector, optimized optics, and low noise analog signal processing to detect heart rate signals. Although the sampling rate is up to 1000 samples per second, after testing different sampling rates, we set it to 400 samples per second having high measurement accuracy with smaller data storage files and faster processing speed. Furthermore, the MAX30100 includes a proprietary discrete time filter to reject 50 Hz interference and low-frequency residual ambient noise. The second part includes the ATMEL ATmega8L, a low-power CMOS 8-bit microcontroller based on the AVR RISC architecture. It was programmed to collect the raw data from the sensor module and transfer them to the laptop via Bluetooth communication.

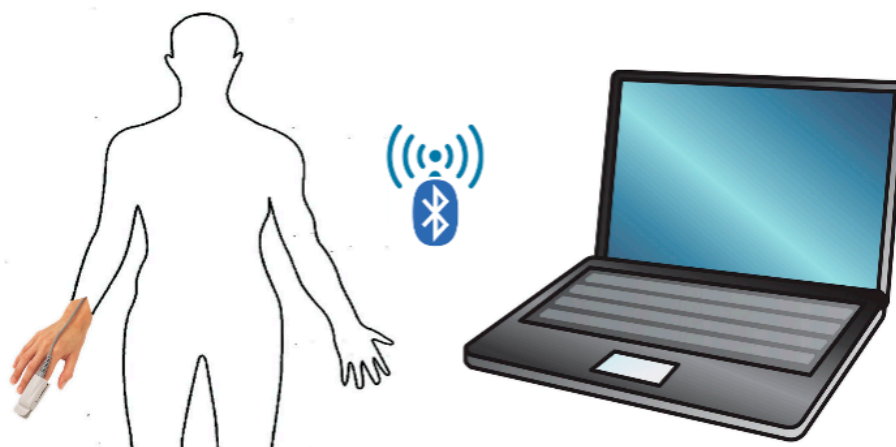


Figure 2. Connectivity of the prototype photoplethysmography (PPG) system.

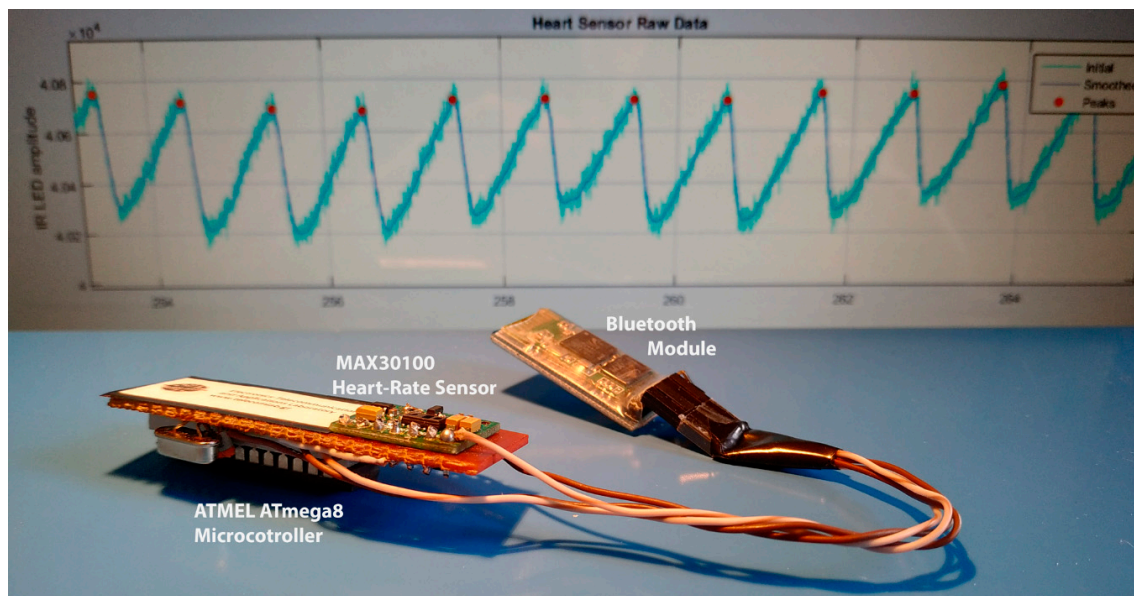


Figure 3. Prototype photoplethysmography electronic device.

2.3. Signal Processing

QRS complex is the most prominent ECG wave for signal analysis and the accurate detection of its R peak is essential for the ECG analysis algorithms [25]. Figure 4 illustrates an ECG signal from a healthy individual's body which was taken from the conventional system.

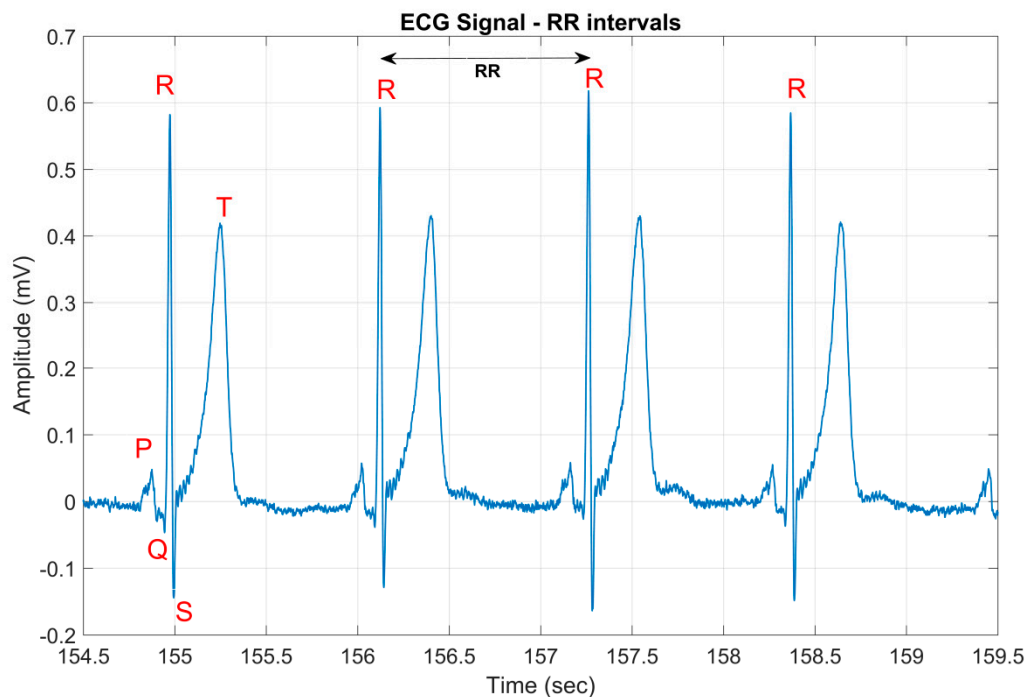


Figure 4. Captured ECG signal (healthy male, 34 years old).

The idea of PPG technique is simple and requires a light source, especially Infrared Light Emitting Diode (IR-LED) or a red LED, which illuminates the tissue such as finger, earlobe, and forehead [26]. A photodetector measures the intensity variations of reflected or transmitted light from the blood volume variation in the tissue [27]. Figure 5 illustrates a typical PPG signal that was captured from PPG sensor

that was placed on the index finger of a healthy 34 year old male. It has a triangular shape with two peaks and for our convenience the upper peak was labeled as P peak-pulse.

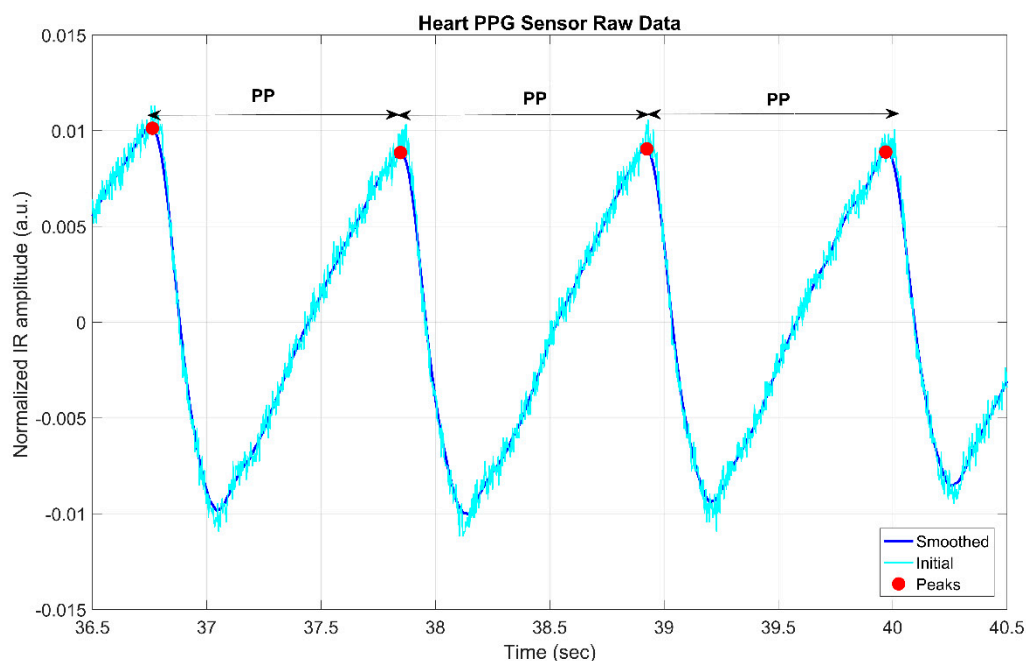


Figure 5. Captured PPG signal (healthy male, 34 years of age).

Before analyzing the time series of RR and PP intervals with NTA, we needed to determine the R peaks from the ECG signal and the P peaks from the PPG signal. For the case of the ECG signal, we used the Pan-Tomkins algorithm which is a well-known technique for detection of the QRS complex [28,29].

The PPG signal is simpler as mentioned above with an upward and a downward peak. Hence, the upper P peak detection algorithm contains fewer steps.

Figure 6 shows the block diagram of the PPG technique. The algorithm for the detection of the P peaks includes the following steps: first, we applied a moving average window for smoothing the signal. The data were smoothed using a moving average filter. The filter had 40 points corresponding to time length of 0.1 s, as the sampling rate was 400 sps. As the volunteers were in resting stage, without e.g., muscle movements, the PPG signal-to-noise ratio was high, and the algorithm used only a smoothing code to eliminate the extra noise spikes. Next, we applied a code searching for local maxima, i.e., finding a peak inside a small frame of time, usually 0.5 s, in which we expected only one P peak. After testing different sampling rates, we concluded that we had the best accuracy speed at 400 samples per second.

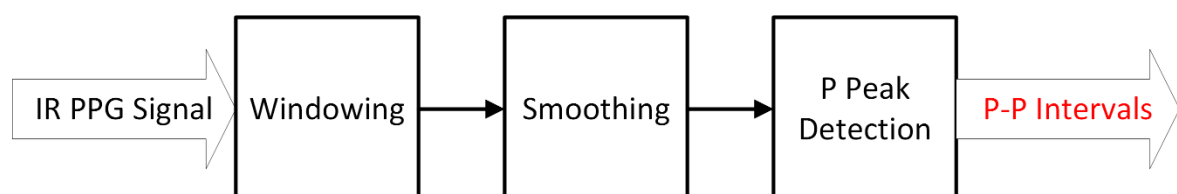


Figure 6. Block diagram of the PPG technique.

Using the above procedure, we obtained the time series for R and P peaks. The time series of R-R and the P-P intervals were calculated by subtracting time values of successive peak occurrences.

2.4. Natural Time Analysis

Natural Time analysis, introduced by Varotsos, Sarlis, and Skordas in 2001 [13], identifies when a dynamical complex system, like the human heart, approaches a phase change (critical point), like SCD, and it can provide information about the moment that this event will occur. The NTA analyzes the series of sequential events each of which is a pair (χ_k, Q_k) (see below), where χ_k corresponds to the order of the event and Q_k to the energy. In the case of ECG the energy of the events is approximately quantified by the distances, e.g., RR of the ECG. NTA provides information by studying the events without caring about the conventional time that they occurred but by keeping their order of occurrence [13,21].

Figure 7 illustrates an example of converting a conventional ECG signal to NTA. The quantity Q_m is quantified to a first approximation by the distance between two consecutive R peaks in the conventional time (Figure 7a). The reading in NTA is indicated in Figure 7b where the length of each RR distance corresponds to the energy of the event on the vertical axis, while on the horizontal axis the events are placed equidistant in the same sequence that they appeared (see Chapter 2 of [13]). Thus, the three distances Q_m , Q_{m+1} , and Q_{m+2} correspond to three events with their respective energy. In the conventional time the ECG reading upon time reversal is plotted in Figure 7c. By the same procedure, we converted it to NTA upon time reversal in Figure 7d. In other words, the last event becomes first, the penultimate second, and so on [13].

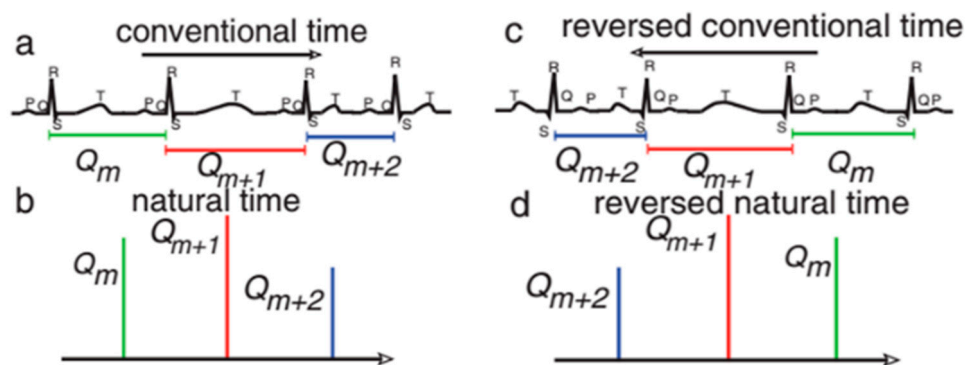


Figure 7. (a) ECG in which the RR distances are marked; (b) the same ECG plotted in (a) but read in Natural Time Analysis (NTA); (c) ECG at conventional time upon time reversal; (d) ECG upon time reversal in NTA.

At this point we will give the definition of natural time which is symbolized as χ by the Greek word “χρόνος”. If we consider a set of events consisting of N events (heartbeats) then the natural time is defined as $\chi_k = k/N$ where the k index defines the k -th event from the total N events. An additional fact studied is the quantity Q_k which defines the energy of the k -th event and in the case of ECG is approximately quantified by the distance of the two consecutive R peaks [13,23] as already mentioned.

According to the above, we define the measure

$$p_k = \frac{Q_k}{\sum_{n=1}^N Q_n}, \quad (1)$$

which expresses the percentage of energy emitted in the k -event in relation to the total energy. Obviously, the sum of all the ratios of the energies will be equal to the unit, namely

$$\sum_{k=1}^N p_k = 1. \quad (2)$$

The entropy is defined in NTA by the relation

$$S = \sum_{k=1}^N \frac{k}{N} \ln\left(\frac{k}{N}\right) p_k - \left(\sum_{k=1}^N \frac{k}{N} p_k \right) \ln\left(\sum_{k=1}^N \frac{k}{N} p_k \right), \quad (3)$$

or equivalently as:

$$S \equiv \langle \chi \ln \chi \rangle - \langle \chi \rangle \ln \langle \chi \rangle. \quad (4)$$

The symbol

$$\langle f(\chi) \rangle \equiv \sum_{k=1}^N f(\chi_k) p_k \quad (5)$$

indicates the average value with respect to the measure p_k . In essence, NTA studies the evolution of the couples (χ_k, Q_k) or (χ_k, p_k) . NTA considers also the time inversion of the sequences of the RR and PP time series, which means that, the last becomes first, the penultimate second, and so forth, as already mentioned above. This is done with the time inversion operator \hat{T} , so for the quantities Q_k and p_k we have

$$\hat{T}Q_k = Q_{N-k+1} \text{ and} \quad (6)$$

$$\hat{T}p_k = p_{N-k+1}, \quad (7)$$

respectively.

We define the entropy under time reversal as:

$$S_- \equiv \langle \chi \ln \chi \rangle_T - \langle \chi \rangle_T \ln \langle \chi \rangle_T = \sum_{k=1}^N \frac{k}{N} \ln\left(\frac{k}{N}\right) p_{N-k+1} - \left(\sum_{k=1}^N \frac{k}{N} p_{N-k+1} \right) \ln\left(\sum_{k=1}^N \frac{k}{N} p_{N-k+1} \right). \quad (8)$$

The entropy change

$$\Delta S \equiv S - S_- \quad (9)$$

gives us useful information in the study of complex systems that operate far away from the equilibrium state, as is the case of the heart [30] and enables the distinction of healthy individuals from those who suffer from heart disease [24,31]. We clarify that living systems are examples of systems operating far from equilibrium which could be understood as follows (e.g., see [32,33] and references therein): living systems are subject to mass, energy, entropy, and information fluxes across their boundaries. Time irreversibility, which is fundamental property of far from equilibrium systems, is related to the unidirectionality of the energy flow across the boundaries of the system. In contrast, processes under equilibrium conditions are time reversible, and hence states approaching death are expected to be more time reversible than those representing far from equilibrium healthy physiology (cf. death is a state of maximum equilibrium since there are no driving forces or consumption of energy). On such a basis in [13] the SCD was considered as phase change (dynamic phase transition), which inspired that NTA could be applied to the distinction between H and SCD.

To distinguish similar-looking electrical signals that are “emitted” from dynamical systems that are far from their equilibrium state, the NTA uses complexity measures. Some of them employ the standard deviation δS which is computed in a discrete window consisting of a number of pulse-events e.g., three pulses, sliding by one event-pulse each time on the ECG. It has been proven that the study of the standard deviation δS of the entropy at a moving window of fixed number of events can distinguish healthy humans from individuals who suffered from cardiac diseases (for a review see Chapter 9 of [13]).

Now we define the complexity measures associated with the ratio of the standard deviation σ of the entropy change ΔS . For short scales, e.g., seven R or P pulses, the complexity measure is equal to

$$\Lambda_7(\tau) = \frac{\sigma[\Delta S_7(\tau)]}{\sigma[\Delta S_3(\tau)]}, \quad (10)$$

where the subscript denotes the number of pulses considered into the calculation and the symbol τ corresponds to the RR, or PP pulses intervals. For large scales, e.g., 49 R or P pulses is equal to

$$\Lambda_{49}(\tau) = \frac{\sigma[\Delta S_{49}(\tau)]}{\sigma[\Delta S_3(\tau)]}. \quad (11)$$

The selection of scales here was made on the basis that when analyzing intervals of long-duration ECG recordings, the combination of $\sigma[\Delta S_7]$ with Λ_7 and Λ_{49} enables the ternary distinction in healthy, SCD and congestive heart failure (CHF) individuals [20,24,31]. To shed more light on the selected number of RR intervals (3, 7, and 49 intervals) involved in the definition of the aforementioned complexity measures, we considered (see [21] and references therein) that physiologically, the origin of the complex dynamics of heart rate has been attributed to antagonistic activity of the two branches of the autonomic nervous system (i.e., the parasympathetic and the sympathetic nervous systems, decreasing and increasing heart rate [34–37], respectively) and that a variety of research has established [38] two clear frequency bands in heart rate and blood pressure with autonomic involvement: (i) a high frequency band, which lies in [39,40] the range 0.15–0.40 Hz and is [35] “indicative of the presence of respiratory modulation of the heart rate” or reflects [40] “modulation of vagal activity, primarily by breathing” and (ii) a low frequency (LF) band from 0.04 to 0.15 Hz (i.e., at around 0.1 Hz), which is usually described as corresponding to [39] “the process of slow regulation of blood pressure and heart rate” or that [40] “it reflects modulation of sympathetic or parasympathetic activity by baroreflex mechanisms” due to [35] “the emergence of a limit cycle caused by the vascular sympathetic delay” its exact explanation, however, is debated [41]. Moreover, the existence of a very low-frequency band (VLF) in the region 0.003 to 0.04 Hz has been identified [42]. The aforementioned scale of three heartbeats corresponds to the high frequency band whereas the scales of 7 and 49 heartbeats lie near to the transition from the high frequency to the LF band and from the LF band to the VLF band, respectively. In particular, in [21] the authors found that the entropy change ΔS_3 under time reversal, at the scale of three heartbeats (high frequency band), identifies the SCD risk and distinguishes SCD from truly healthy individuals as well as from CHF. Later, in [24] an optimum discrimination between H, CHF, and SCD was achieved by using the scales 3, 7, and 49 heartbeats, which may be considered as extending the results obtained in [21] for the importance of the high frequency and LF band in distinguishing SCD from H by strengthening also the spectral part of the transition region from LF to VLF.

2.5. Clinical Study Protocol—Data Collection

The collection of conventional ECG and PPG recordings was done in the setting of 2nd Department of Cardiology, University Hospital of Ioannina, Ioannina, Greece. This was a prospective study including both chronic HF patients and healthy subjects that was performed during a period of 2 months February–March 2017. Patients with HF who were hospitalized in the department and consented to participate were included in the analysis. The diagnosis of HF was based on currently established criteria proposed by the European Society of Cardiology in most recent published Guidelines [8]. Exclusion criteria were the presence of acute illness other than HF that could determine the short-term prognosis of the patients and the presence of a permanent pacemaker or other implantable cardiac rhythm device that determined the patients’ heart rate/rhythm; patients with cardiac rhythm devices not entirely dependent were included in the analysis. All patients that participated in the study signed an informed consent form based on a clinical protocol approved by local ethics committee.

Over 100 eligible patients hospitalized with HF were screened and finally 67 patients with HF were enrolled in the current study; patients were not enrolled either due to the presence of permanent cardiac pacing (the majority of excluded cases) or the denial to consent for participation (a small minority). Healthy participants were selected among the medical and nurse staff of the cardiology department. The measurements took place on the bed of the patients who were lying quiet for 20 min in the supine position. The ECG leads were obtained using three transdermal patches (the same patches were applied to all patients during the study) placed over a bone formation: two on the upper right and left thorax and one over the lower ribs. At the same time the PPG signals were recorded using the relevant device applied usually to the right index figure. For all patients, data regarding personal medical history, current medications, and recent biochemical/metabolic profile were recorded. The measurements of healthy subjects were performed in a quiet room with the same methodology as described above for HF patients.

2.6. Receiver Operating Characteristics (ROC) Method

A Receiver Operating Characteristics (ROC) diagram depicts the hit rate (or True positive rate) versus false alarm rate (or False positive rate) thus showing the trade-off between hits and false alarms [43]: the hit rate (h) is the ratio of the True Positives (TP) over the totality of Positive (P) cases, $h = TP/P$, while false alarm rate (f) is the ratio of False Positives (FP) over the totality of Negative cases Q, $f = FP/Q$. Since h and f are in general independent, ROC diagrams can provide information for the quality of a selection scheme. The statistical significance of such a scheme depends on the Area Under the Curve (AUC) obtained when we vary the selection threshold. Recently, a method has been proposed [44] that can estimate the AUC—and hence the statistical significance—corresponding to an operating point of the ROC based on confidence ellipses.

2.7. Support Vector Machines (SVM)

Support Vector Machines (SVM) [45–50] is a learning machine that can be used for two-group classification even for non-separable data which also avoids computing posterior probabilities. Here, we used the computer code *SMV^{light}* [47,51] using a (Gaussian) radial basis function $K(\vec{a}, \vec{b}) = \exp\left(-\gamma|\vec{a} - \vec{b}|^2\right)$, e.g., see Equation (5.35) on page 145 of [48], for the construction of the decision function

$$f(\vec{x}) = \text{sign}\left\{\sum_{k=1}^l [y_k \alpha_k K(\vec{x}_k, \vec{x})] - b\right\}, \quad (12)$$

e.g., see Equation (5.25) on page 141 of [48]. SVM provide optimally [45,46,48] the number l of the support vectors \vec{x}_k , the weights $y_k \alpha_k$, and the bias b .

3. Results

Our database contains simultaneous ECG and PPG recordings from 32 records from H individuals (nine women and 23 men), aged 24 to 58, and 67 records from patients (22 women and 45 men), aged 55 to 87. Other parameters recorded from patients include the following: age, gender, weight, smoking, arterial hypertension, diabetes mellitus, hyperlipidemia, coronary artery disease, atrial fibrillation, heart failure, syncope, Implantable Cardiac Defibrillator (ICD), pacemaker implantation, family history of sudden cardiac death. Furthermore, a series of these records include laboratory blood testing results as well as the medication history. After data acquisition from both ECG and PPG systems and the completion of the signal processing, including calculation of RR and PP time series, we applied NTA for finding the complexity measures Λ_7 and Λ_{49} for each individual.

It has been demonstrated that the PPG signal can replace the ECG recordings for the extraction of HRV indices, especially in monitoring healthy individuals at rest [52,53]. For proving the similarity

between ECG and PPG signals, we took the RR and PP intervals from our recorders for a randomly chosen healthy subject, and applied the transparent histogram, as shown in Figure 8. The recording time was 20 min and the number of samples was 1117 for each case. As shown in Figure 8, both signals result in histograms that are close. The mean value for ECG was 1.073 s and 1.073 s for PPG while the standard deviation for ECG was 0.033 s and 0.036 s for PPG.

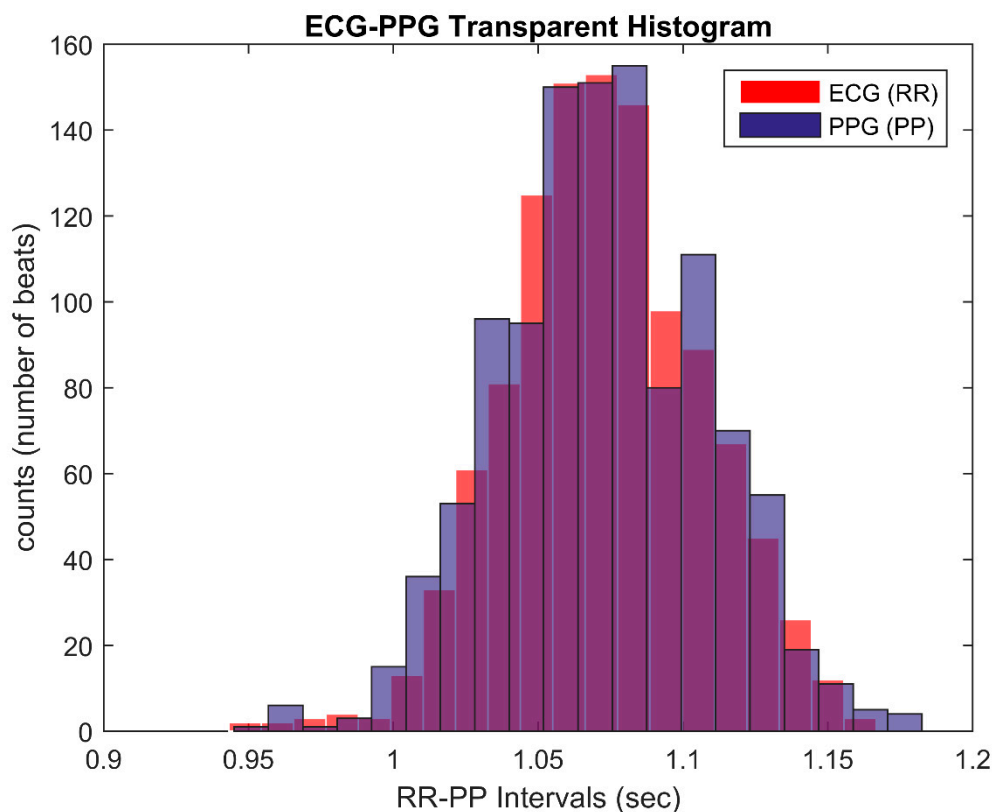


Figure 8. RR and PP intervals for a randomly chosen healthy subject.

We performed *t*-test analyses (one sample, paired samples *t*-test and independent samples *t*-test). Specifically, for the one-sample test (Table 1) the *p*-value for each group was found below 0.05 (Sig. (two-tailed) = 0.000). This type of *t*-test compares each groups' mean value with a predefined mean value which was selected to be the typical value of zero in both cases. The paired samples *t*-test (Table 2) confirmed that the correlation of their mean values is high with a *p*-value of less than 0.05 (Sig. = 0.000). Finally, the independent samples *t*-test, see Table 3, pointed to the validity of high correlation between the mean values. In particular, we found that the mean values are strongly correlated with each other since the *p*-value was >0.05 (Sig. = 0.975) which evidently does not reject the null hypothesis (no significant difference between compared groups).

Table 1. One-sample test.

	t	df	Sig. (Two-Tailed)	Mean Difference	95% Confidence Interval of the Difference	
					Lower	Upper
ECG (RR)	1077.070	1116	0.000	1.07295859	1.0710040	1.0749132
PPG (PP)	991.153	1116	0.000	1.0729118	1.070788	1.075036

Table 2. Paired samples correlations.

	N	Correlation	Sig.
ECG (RR) and PPG (PP)	1117	0.825	0.000

Table 3. Independent samples test.

	F	Sig.	t	df	Sig. (Two-Tailed)	Mean Difference	Std. Error Difference
	Levene's Test for Equality of Variances		t-Test for Equality of Means				
Equal variances assumed	8.059	0.005	0.032	2232	0.975	0.00004678	0.00147111
Not equal variances assumed			0.032	2216.767	0.975	0.00004678	0.00147111

Figure 9 depicts the complexity measures Λ_7 and Λ_{49} for all individuals with the PPG technique. We set two threshold lines: a vertical $[\Lambda_7]_c$ straight line with value $\Lambda_7 = 1.55$ and a horizontal $[\Lambda_{49}]_c$ straight line with value $\Lambda_{49} = 1.48$. We observe that the vast majority of H lies in the right of the $[\Lambda_7]_c$ line and above the $[\Lambda_{49}]_c$ line. Especially, only three of the 32 healthy individuals are mixed with CHF. On the other hand, 13 CHF are mixed with H. The sensitivity s (the proportion of the truly identified positives) in each of the two regions, for the H region when the $\Lambda_7 > [\Lambda_7]_c$ and $\Lambda_{49} > [\Lambda_{49}]_c$, is $s_H = 90\%$. Hereafter, this region is called the H region. In the remaining region (hereafter called the CHF region), we had sensitivity $s_{CHF} = (67-13)/67 = 80.6\%$.

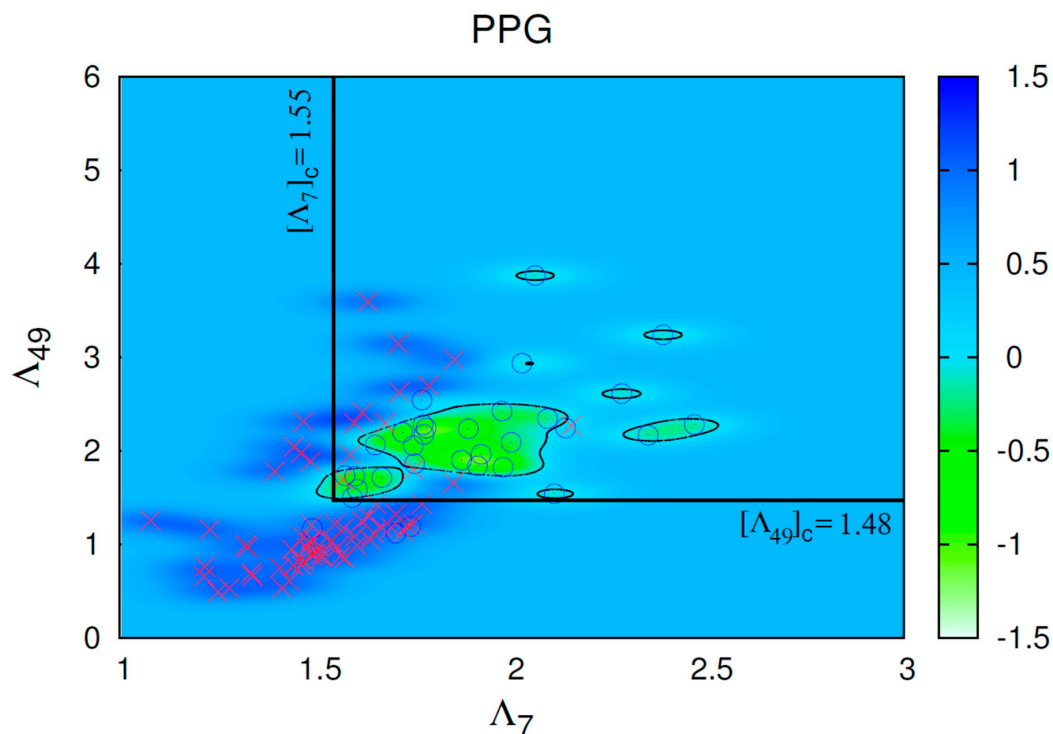


Figure 9. Results comprising 32 Healthy (blue circles) and 67 congestive heart failure (CHF) (red crosses) individuals. The color contours correspond to the argument of the signum in the decision function of Equation (12) obtained by Support Vector Machines (SVM) with radial basis kernel function with $\gamma = 50$. The black dotted points correspond to the decision boundary and enclose the healthy (H) region found by SVM.

Figure 10 depicts the complexity measure Λ_7 and Λ_{49} for all individuals depicted in Figure 9 but with the ECG technique. We notice that the points, especially those of H, moved to the top right, compared to the PPG diagram.

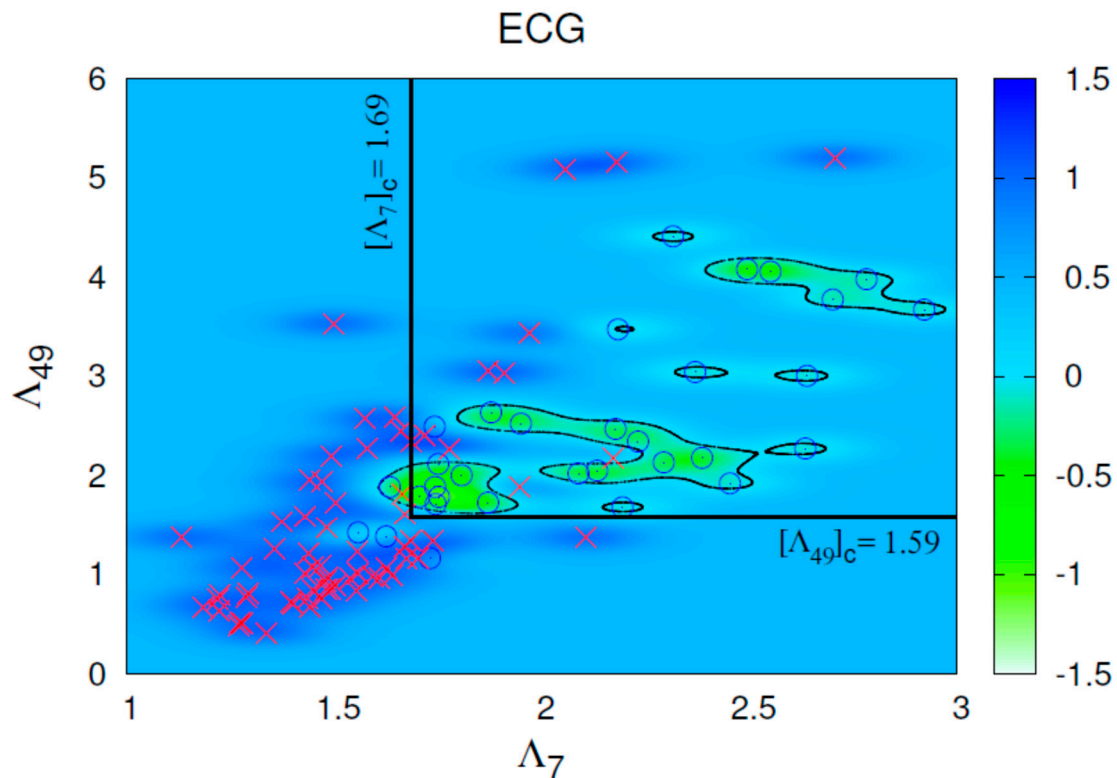


Figure 10. Results comprising 32 Healthy (blue circles) and 67 CHF (red crosses) individuals. The color contours correspond to the argument of the signum in the decision function of Equation (12) obtained by SVM with radial basis kernel function with $\gamma = 60$. The black dotted points correspond to the decision boundary and enclose the H region found by SVM.

We again set two threshold lines: a vertical $[\Lambda_7]_c$ line with value $\Lambda_7 = 1.69$ and a horizontal $[\Lambda_{49}]_c$ line with value $\Lambda_{49} = 1.59$ and the sensitivity s was calculated in the same way as previously. An inspection of this figure shows that the vast majority of H (i.e., 28 out of 32) lies in the right of the $[\Lambda_7]_c$ line and above the $[\Lambda_{49}]_c$ line. Hence, in this region sensitivity $s_H = 87.5\%$. This is the H region. In the remaining region, we found the vast majority of CHF, i.e., 56 out of 67, thus the sensitivity for CHF was $s_{CHF} = 83.5\%$ (and only four H are mixed with CHF). This is the CHF region.

In order to confirm statistically the differences between the two groups of H and CHF patients, we performed an independent samples t -test comparing the means of the groups. Our sample, for both groups, follows the normal distribution according to the Shapiro–Wilk normality test. The independent t -test results are summarized in Tables 4 and 5. The results indicate that there are statistically significant differences for the parameters Λ_7 ($p = 0.000$) and Λ_{49} ($p = 0.000$), between the H and CHF individuals measured by the PPG method. Similar results are obtained for the method of ECG measurements as they are shown in Tables 6 and 7.

Table 4. Group statistics for the H subjects and CHF patients (PPG method).

Parameter	Group	n	Mean	Std. Deviation	Std. Error Mean
Λ_7	Healthy	32	1.888	0.251	0.044
	CHF	67	1.539	0.177	0.022
Λ_{49}	Healthy	32	2.085	0.573	0.101
	CHF	67	1.337	0.678	0.083

Table 5. Independent samples *t*-test for the groups of the H subjects and CHF patients (PPG method).

Parameter.	t	df	Sig. (Two-Tailed)	Mean Difference	Std. Error Difference	95% Confidence Interval of the Difference	
						Lower	Upper
Λ_7	7.049	46.166	0.000	0.348	0.049	0.249	0.448
Λ_{49}	5.381	97.000	0.000	0.748	0.139	0.472	1.023

Table 6. Group statistics for the H subjects and CHF patients (ECG method).

Parameter	Group	n	Mean	Std. Deviation	Std. Error Mean
Λ_7	Healthy	32	2.127	0.389	0.069
	CHF	68	1.567	0.270	0.033
Λ_{49}	Healthy	32	2.474	0.891	0.157
	CHF	68	1.566	1.069	0.130

Table 7. Independent samples *t*-test for the groups of the H subjects and CHF patients (ECG method).

Parameter	t	df	Sig. (Two-Tailed)	Mean Difference	Std. Error Difference	95% Confidence Interval of the Difference	
						Lower	Upper
Λ_7	7.355	45.626	0.000	0.560	0.076	0.407	0.713
Λ_{49}	4.167	98.000	0.000	0.908	0.218	0.475	1.340

The statistical significance of the separation between CHF and H obtained by means of $[\Lambda_7]_c$ and $[\Lambda_{49}]_c$ in Figures 9 and 10 when using PPG and ECG data, respectively, can be estimated by means of the ROC method. A ROC diagram depicting the results obtained by either PPG or ECG data is shown in Figure 11. In Figure 11, we estimated the *p*-value to obtain, by chance, the aforementioned classification scheme using the computer code VISROC available from [44] and obtained values well below 0.01%. Concerning the AUC for PPG and ECG data, they are very close one to another since we obtained 0.953 and 0.954, respectively.

In an attempt to obtain a better classification between CHF and H, we also employed the method of SVM [45–51]. When the decision function of Equation (12) equaled +1 we assigned the point with coordinates $\vec{x} = (\Lambda_7, \Lambda_{49})$ to CHF, while when it equaled −1 to H. In Figures 9 and 10, the color contours correspond to the argument of the signum in the decision function of Equation (12). We varied γ in order to obtain the maximum accuracy *A* which is the ratio of the sum of TP plus True Negatives (TN) over the totality of the cases examined, $A = (TP + TN)/(P + Q)$: for $\gamma = 50$ we obtained for PPG the value $A = 93\%$ (one CHF mixes with H and six H mix with CHF, see the contours in Figure 9), while for $\gamma = 60$ we obtained for ECG the value $A = 95\%$ (one CHF mixes with H and four H mix with CHF, see the contours in Figure 10).

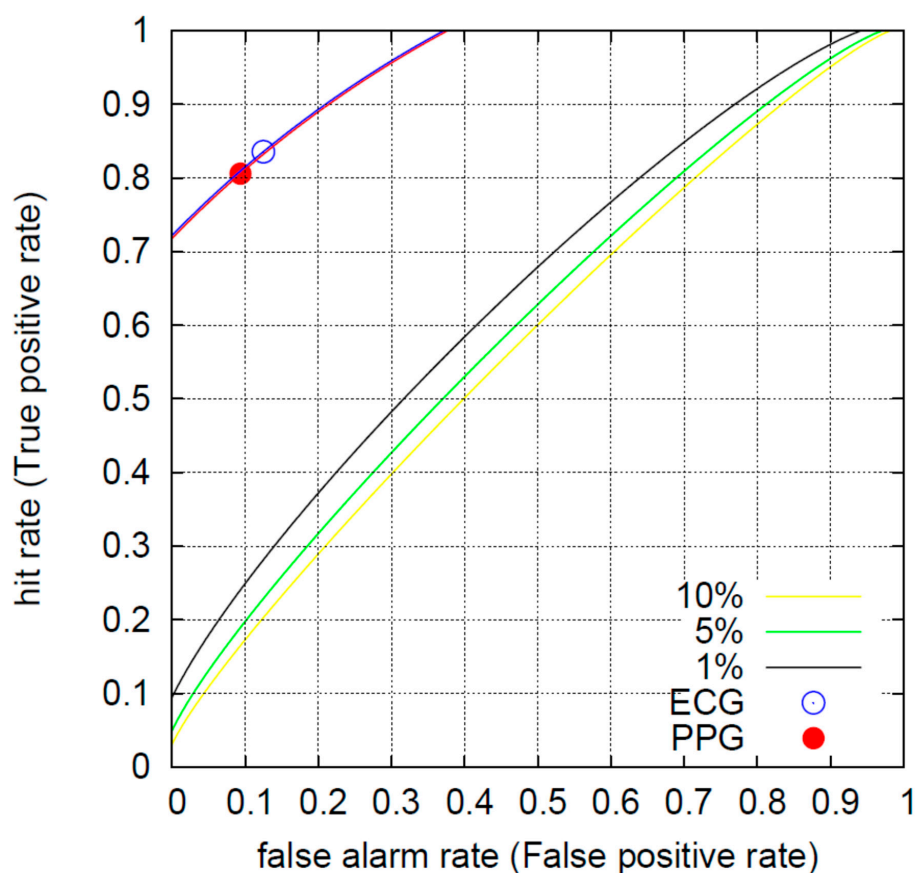


Figure 11. Receiver Operating Characteristics (ROC) diagram depicting the operating points when using PPG (red filled circle) or ECG (blue open circle) data according to the separation between CHF and H obtained by means of $[\Lambda_7]_c$ and $[\Lambda_{49}]_c$ in Figures 10 and 11, respectively, together with the corresponding ROC curves (red and blue, respectively) estimated on the basis of confidence ellipses [44]. The other three curves (yellow, green, black) correspond to the p -values 10%, 5%, 1%, respectively, when 67 (= P) CHF individuals are to be selected out of 99 (= P + Q) cases [44]. The p -values obtained for both PPG and ECG are well below 0.01% while the corresponding AUC are 0.953 and 0.954, respectively.

4. Discussion and Conclusions

Previous ECG-based methods for automated computer aided detection (CAD) of HF using various methodologies have achieved encouraging results. The duration of ECG signal recording was variable and could be as short as 2 s [10,54–58]. Simple clinical prediction rules (CPR) for HF detection performed less well compared to ECG based methods [59]. The addition of clinical parameters and natriuretic peptides on ECG-derived signals may improve HF detection algorithms [10]. To compare our present results with studies of other groups to distinguish a target group comprising a considerable number of CHF, say 40 or more, from healthy individuals, we compile in Table 8 the most recent CAD systems using HRV and the most recent systematic review [59] of CPR for the diagnosis of HF. An inspection of this table reveals that the sensitivity values achieved in the present study is comparable to the highest values reported to date.

Turning now to NTA studies, earlier work was undertaken by using ECG (see Table 9) and revealed promising results concerning the distinction between H and CHF by means of the complexity measures Λ_7 and Λ_{49} . Future studies could assess the role of adding clinical parameters and biomarker data in improving the accuracy for HF detection.

Table 8. Comparison of the present study with the most recent computer aided detection (CAD) systems using Heart Rate Variability (HRV) and the clinical studies discussed in the most recent review [59] to distinguish CHF from H. (LF/HF: LF over high frequency ratio of power spectral density, BNP: B-type natriuretic peptide, MICE: Male, infarction, crepitations, edema).

Reference	Parameters Used	Sensitivity s_{CHF}
Hua et al. [9] (see Table 8)	Various HRV classifiers	85.37% to 97.56%
Pan et al. [60] (see Table 3)	Multi-Frequency Components Entropy (or LF/HF)	63.6% to 79.5% (or 86.4%)
Gallagher et al. [59] (see Table 4)	BNP alone	75.6% to 84.7%
Roalfe et al. [61]	MICE, MICE and ECG, MICE and BNP, MICE and ECG and BNP	58.5% to 86.2% (see Table 4 of [59])
Fahey et al. [62]	CPR, CPR and ECG, CPR and BNP, CPR and ECG and BNP	55.3% to 86.2% (see Table 4 of [59])
Boonman-de Winter et al. [63]	Clinical score	67.7% to 75.6% (see Table 4 of [59])
Yamamoto et al. [64]	Clinical score (and BNP)	54.2% to 76.1% (see Table 4 of [59])
This work	$\Lambda_7(PP)$, $\Lambda_{49}(PP)$	80.6% (97.7% when employing SVM)
	$\Lambda_7(RR)$, $\Lambda_{49}(RR)$	83.5% (97.7% when employing SVM)

Table 9. Comparison of the previous NTA studies for the distinction of CHF patients from H and SCD individuals with the present NTA study. (In this table: NN refers to NN intervals between consecutive normal beats, while intervals between pairs of normal beats surrounding an ectopic beat are discarded; N_3 is the ratio $\sigma[\Delta S_3^{shuf}]/\sigma[\Delta S_3]$, where the superscript *shuf* denotes that ΔS_3^{shuf} time-series is calculated upon randomly shuffling the original NN time-series [21]).

Reference	Parameters Used	Sensitivity s_{CHF}
Varotsos et al. [21] (see Figure 3a)	$N_3(NN)$, $\sigma[\Delta S_7](NN)$	61.4%
Sarlis et al. [24] (see Table 1)	$\Lambda_7(NN)$, $\Lambda_{49}(NN)$, $\sigma[\Delta S_3](NN)$	68.2%
This work	$\Lambda_7(PP)$, $\Lambda_{49}(PP)$	80.6% (97.7% when employing SVM)
	$\Lambda_7(RR)$, $\Lambda_{49}(RR)$	83.5% (97.7% when employing SVM)

In this paper, we employed NTA in the dynamical system of the heart by using data obtained both by a prototype low-cost portable PPG electronic device as well as by ECG and compared the results. In particular, the results obtained by PPG show that these complexity measures for 99 individuals exhibit 90% sensitivity for the H region and 81% for the CHF region. Moreover, these results indicate that there are statistically significant differences for Λ_7 and Λ_{49} between the H and CHF individuals measured either by the prototype PPG electronic device or by the conventional ECG system. The statistical significance is further strengthened by employing ROC diagrams (Figure 11) which reveal more or less the same value of AUC for both PPG and ECG. In addition, the classification between CHF and H was elaborated by using non-linear radial basis function SVM (see the color contours in Figures 9 and 10) that led to comparable values of accuracy A for both PPG and ECG. The competitive advantages for the new prototype electronic device include the low-cost, the portability and the few minutes time window to produce clear results. No previous study has reported NTA results concerning the distinction of HF from H by means of PPG signals. Further improvement of the prototype PPG electronic device requires data processing and NTA in real time. We expect that the employment of this PPG electronic device in the general population due to its simplicity of use could contribute to the detection of underlying heart problems and the timely notification to health care units.

Author Contributions: Conceptualization, P.K., P.V., N.V.S., E.S.S.; methodology, G.B., V.C., G.T., K.K.N., A.B., L.K.M.; software, G.B., G.T., V.C., S.K.C.; validation, N.V.S. and E.S.S.; data curation, G.B., K.K.N., A.B.; writing—original draft preparation, G.B., V.C., G.T.; writing—review and editing, P.V., N.V.S., E.S.S., S.K.C.; supervision, D.P.; project administration, P.K.

Funding: This research received no external funding.

Conflicts of Interest: The authors declare no conflict of interest.

References

- Allen, J. Photoplethysmography and its application in clinical physiological measurement. *Physiol. Meas.* **2007**, *28*, R1–R39. [[CrossRef](#)] [[PubMed](#)]
- Tamura, T.; Maeda, Y.; Sekine, M.; Yoshida, M. Wearable Photoplethysmographic Sensors—Past and Present. *Electronics* **2014**, *3*, 282–302. [[CrossRef](#)]
- Park, S.; Jayaraman, S. Enhancing the Quality of Life Through Wearable Technology. *IEEE Eng. Med. Biol. Mag.* **2003**, *22*, 41–48. [[CrossRef](#)] [[PubMed](#)]
- Elgendi, M. On the Analysis of Fingertip Photoplethysmogram Signals. *Curr. Cardiol. Rev.* **2012**, *8*, 14–25. [[CrossRef](#)] [[PubMed](#)]
- Savarese, G.; Lund, L.H. Global Public Health Burden of Heart Failure. *Card. Fail. Rev.* **2017**, *3*, 7–11. [[CrossRef](#)]
- Giannitsi, S.; Bougiakli, M.; Bechlioulis, A.; Naka, K. Endothelial dysfunction and heart failure: A review of the existing bibliography with emphasis on flow mediated dilation. *JRSM Cardiovasc. Dis.* **2019**, *8*, 2048004019843047. [[CrossRef](#)]
- Han, J.; Trumble, D.R. Cardiac Assist Devices: Early Concepts, Current Technologies, and Future Innovations. *Bioengineering* **2019**, *6*, 18. [[CrossRef](#)]
- Ponikowski, P.; Voors, A.A.; Anker, S.D.; Bueno, H.; Cleland, J.G.F.; Coats, A.J.S.; Falk, V.; González-Juanatey, J.R.; Harjola, V.P.; Jankowska, E.A.; et al. 2016 ESC Guidelines for the diagnosis and treatment of and chronic heart failure: The Task Force for the diagnosis and treatment of acute and chronic heart failure of the European Society of Cardiology (ESC) Developed with the special contribution of the Heart Failure Association (HFA) of the ESC. *Eur. Heart J.* **2016**, *37*, 2129–2200. [[CrossRef](#)]
- Hua, Z.; Chen, C.; Zhang, R.; Liu, G.; Wen, W. Diagnosing Various Severity Levels of Congestive Heart Failure Based on Long-Term HRV Signal. *Appl. Sci.* **2019**, *9*, 2544. [[CrossRef](#)]
- Jahmunah, V.; Oh, S.L.; Wei, J.K.E.; Ciaccio, E.J.; Chua, K.; San, T.R.; Acharya, U.R. Computer-aided diagnosis of congestive heart failure using ECG signals—A review. *Phys. Med.* **2019**, *62*, 95–104. [[CrossRef](#)]
- Baldoumas, G.; Peschos, D.; Tatsis, G.; Votis, C.I.; Chronopoulos, S.K.; Christofilakis, V.; Kostarakis, P.; Sarlis, N.V.; Skordas, E.S.; Naka, K.K.; et al. Comparison of the R-R intervals in ECG and Oximeter signals to be used in complexity measures of Natural Time Analysis. In Proceedings of the 2018 7th International Conference on Modern Circuits and Systems Technologies (MOCAST), Thessaloniki, Greece, 7–9 May 2018. [[CrossRef](#)]
- Zebrowski, J.J.; Poplawska, W.; Baranowski, R.; Buchner, T. Symbolic dynamics and complexity in a physiological timeseries. *Chaos Solitons Fractals* **2000**, *11*, 1061–1075. [[CrossRef](#)]
- Varotsos, P.A.; Sarlis, N.V.; Skordas, E.S. *Natural Time Analysis: The New View of Time*; Springer: Berlin/Heidelberg, Germany, 2011.
- Varotsos, P.A.; Sarlis, N.V.; Skordas, E.S. Long-range correlations in the electric signals that precede rupture. *Phys. Rev. E* **2002**, *66*, 011902. [[CrossRef](#)] [[PubMed](#)]
- Varotsos, P.A.; Sarlis, N.V.; Skordas, E.S.; Lazaridou, M.S. Fluctuations, under time reversal, of the natural time and the entropy distinguish similar looking electric signals of different dynamics. *J. Appl. Phys.* **2008**, *103*, 014906. [[CrossRef](#)]
- Lazaridou-Varotsos, M.S. *Earthquake Prediction by Seismic Electric Signals*; Springer: Berlin/Heidelberg, Germany, 2013.
- Varotsos, P.A.; Sarlis, N.V.; Skordas, E.S.; Lazaridou, M.S. Seismic Electric Signals: An additional fact showing their physical interconnection with seismicity. *Tectonophysics* **2013**, *589*, 116–125. [[CrossRef](#)]

18. Varotsos, P.A.; Sarlis, N.V.; Skordas, E.S.; Tanaka, H.K.; Lazaridou, M.S. Attempt to distinguish long-range temporal correlations from the statistics of the increments by natural time analysis. *Phys. Rev. E* **2006**, *74*, 021123. [\[CrossRef\]](#) [\[PubMed\]](#)
19. Sarlis, N.V.; Varotsos, P.A.; Skordas, E.S. Flux avalanches in $\text{YBa}_2\text{Cu}_3\text{O}_{7-x}$ films and rice piles: Natural time domain analysis. *Phys. Rev. B* **2006**, *73*, 054504. [\[CrossRef\]](#)
20. Varotsos, P.A.; Sarlis, N.V.; Skordas, E.S.; Lazaridou, M.S. Natural entropy fluctuations discriminate similar-looking electric signals emitted from systems of different dynamics. *Phys. Rev. E* **2005**, *71*, 011110. [\[CrossRef\]](#)
21. Varotsos, P.A.; Sarlis, N.V.; Skordas, E.S.; Lazaridou, M.S. Identifying sudden cardiac death risk and specifying its occurrence time by analyzing electrocardiograms in natural time. *Appl. Phys. Lett.* **2007**, *91*, 064106. [\[CrossRef\]](#)
22. Sarlis, N.V.; Skordas, E.S.; Varotsos, P.A. Heart rate variability in natural time and $1/f$ “noise”. *EPL* **2009**, *87*, 18003. [\[CrossRef\]](#)
23. Varotsos, P.A.; Sarlis, N.V.; Skordas, E.S.; Lazaridou, M.S. Entropy in the natural time domain. *Phys. Rev. E* **2004**, *70*, 011106. [\[CrossRef\]](#)
24. Sarlis, N.V.; Christopoulos, S.-R.G.; Bemplidaki, M.M. Change ΔS of the entropy in natural time under time reversal: Complexity measures upon change of scale. *EPL* **2015**, *109*, 18002. [\[CrossRef\]](#)
25. Tun, H.M.; Moe, W.K.; Naing, Z.M. Analysis of Computer Aided Identification System for ECG Characteristic Points. *Int. J. Biomed. Sci. Eng.* **2015**, *3*, 49–61. [\[CrossRef\]](#)
26. Moraes, J.L.; Rocha, M.X.; Vasconcelos, G.G.; Vasconcelos Filho, J.E.; de Albuquerque, V.H.C.; Alexandria, A.R. Advances in Photoplethysmography Signal Analysis for Biomedical Applications. *Sensors* **2018**, *18*, 1894. [\[CrossRef\]](#) [\[PubMed\]](#)
27. Jayadevappa, B.M.; Holi, M.S. Photoplethysmography: Design, Development, Analysis and Applications in Clinical and Physiological Measurement—A Review. *Int. J. Innov. Res. Sci. Eng. Technol.* **2016**, *5*, 3519–3531. [\[CrossRef\]](#)
28. Sedghamiz, H. *Matlab Implementation of Pan Tompkins ECG QRS Detector*; DataCite: Cambridge, UK, 2014. [\[CrossRef\]](#)
29. Pan, J.; Tompkins, W.J. A Real-Time QRS Detection Algorithm. *IEEE Trans. Biomed. Eng.* **1985**, *BME-32*, 230–236. [\[CrossRef\]](#)
30. Goldberger, A.L.; Amaral, L.A.N.; Hausdorff, J.M.; Ivanov, P.C.; Peng, C.-K.; Stanley, H.E. Fractal dynamics in physiology: Alterations with disease and aging. *Proc. Natl. Acad. Sci. USA* **2002**, *99*, 2466–2472. [\[CrossRef\]](#) [\[PubMed\]](#)
31. Sarlis, N.V. Entropy in Natural Time and the Associated Complexity Measures. *Entropy* **2017**, *19*, 177. [\[CrossRef\]](#)
32. Costa, M.; Goldberger, A.L.; Peng, C.-K. Broken Asymmetry of the Human Heartbeat: Loss of Time Irreversibility in Aging and Disease. *Phys. Rev. Lett.* **2005**, *95*, 198102. [\[CrossRef\]](#)
33. Costa, M.; Peng, C.-K.; Goldberger, A.L. Multiscale Analysis of Heart Rate Dynamics: Entropy and Time Irreversibility Measures. *Cardiovasc. Eng.* **2008**, *8*, 88–93. [\[CrossRef\]](#)
34. Peng, C.-K.; Mietus, J.; Hausdorff, J.M.; Havlin, S.; Stanley, H.E.; Goldberger, A.L. Long-range anticorrelations and non-Gaussian behavior of the heartbeat. *Phys. Rev. Lett.* **1993**, *70*, 1343. [\[CrossRef\]](#)
35. Kotani, K.; Struzik, Z.R.; Takamasu, K.; Stanley, H.E.; Yamamoto, Y. Model for complex heart rate dynamics in health and diseases. *Phys. Rev. E* **2005**, *72*, 041904. [\[CrossRef\]](#) [\[PubMed\]](#)
36. Ivanov, P.C.; Amaral, L.A.N.; Goldberger, A.L.; Stanley, H.E. Stochastic feedback and the regulation of biological rhythms. *Europhys. Lett.* **1998**, *43*, 363. [\[CrossRef\]](#) [\[PubMed\]](#)
37. Amaral, L.A.N.; Ivanov, P.C.; Aoyagi, N.; Hidaka, I.; Tomono, S.; Goldberger, A.L.; Stanley, H.E.; Yamamoto, Y. Behavioral-Independent Features of Complex Heartbeat Dynamics. *Phys. Rev. Lett.* **2001**, *86*, 6026. [\[CrossRef\]](#) [\[PubMed\]](#)
38. Malpas, S.C. Neural influences on cardiovascular variability: Possibilities and pitfalls. *Am. J. Physiol. Heart Circ. Physiol.* **2002**, *282*, H6. [\[CrossRef\]](#) [\[PubMed\]](#)
39. Prokhorov, M.D.; Ponomarenko, V.I.; Gridnev, V.I.; Bodrov, M.B.; Bespyatov, A.B. Synchronization between main rhythmic processes in the human cardiovascular system. *Phys. Rev. E* **2003**, *68*, 041913. [\[CrossRef\]](#)

40. Bigger, J.T., Jr.; Fleiss, J.L.; Steinman, R.C.; Rolnitzky, L.M.; Schneider, W.J.; Stein, P.K. RR Variability in Healthy, Middle-Aged Persons Compared with Patients With Chronic Coronary Heart Disease or Recent Acute Myocardial Infarction. *Circulation* **1995**, *91*, 1936–1943. [CrossRef]
41. Mc Sharry, P.E.; Clifford, G.D.; Tarassenko, L.; Smith, L.A. A dynamical model for generating synthetic electrocardiogram signals. *IEEE Trans. Biomed. Eng.* **2003**, *50*, 289–294. [CrossRef]
42. Taskforce of the European Society of Cardiology and the North American Society of Pacing and Electrophysiology. Heart Rate Variability. *Circulation* **1996**, *93*, 1043–1065. [CrossRef]
43. Fawcett, T. An introduction to ROC analysis. *Pattern Recogn. Lett.* **2006**, *27*, 861–874. [CrossRef]
44. Sarlis, N.V.; Christopoulos, S.R.G. Visualization of the significance of Receiver Operating Characteristics based on confidence ellipses. *Comput. Phys. Commun.* **2014**, *185*, 1172–1176. [CrossRef]
45. Cortes, C.; Vapnik, V. Support-vector networks. *Mach. Learn.* **1995**, *20*, 273–297. [CrossRef]
46. Vapnik, V.N. An overview of statistical learning theory. *IEEE Trans. Neural Netw.* **1999**, *10*, 988–999. [CrossRef] [PubMed]
47. Joachims, T. *Advances in Kernel Methods—Support Vector Learning*; Schölkopf, B., Burges, C., Smola, A., Eds.; MIT-Press: Cambridge, MA, USA, 1999; Chapter 11; pp. 169–184.
48. Vapnik, V. *The Nature of Statistical Learning Theory*, 2nd ed.; Springer: New York, NY, USA, 2000; pp. 138–169.
49. Cristianini, N.; Scholkopf, B. Support Vector Machines and Kernel Methods: The New Generation of Learning Machines. *AI Mag.* **2002**, *23*, 31–41. [CrossRef]
50. Lewes, G.H. *Efficient Learning Machines. Theories, Concepts, and Applications for Engineers and System Designers*; Awad, M., Khanna, B., Eds.; Apress: Berkeley, CA, USA, 2015; Chapter 3; pp. 39–66.
51. Joachims, T. SVM^{light} Support Vector Machine Version 6.02. 14 August 2008. Available online: <http://svmlight.joachims.org> (accessed on 10 October 2019).
52. Schäfer, A.; Vagedes, J. How accurate is pulse rate variability as an estimate of heart rate variability?: A review on studies comparing photoplethysmographic technology with an electrocardiogram. *Int. J. Cardiol.* **2013**, *166*, 15–29. [CrossRef] [PubMed]
53. Lu, G.; Yang, F.; Taylor, J.A.; Stein, J.F. A comparison of photoplethysmography and ECG recording to analyse heart rate variability in healthy subjects. *J. Med. Eng. Technol.* **2009**, *33*, 634–641. [CrossRef] [PubMed]
54. Kwon, J.M.; Kim, K.H.; Jeon, K.H.; Kim, H.M.; Kim, M.J.; Lim, S.M.; Song, P.S.; Park, J.; Choi, R.K.; Oh, B.H. Development and Validation of Deep-Learning Algorithm for Electrocardiography-Based Heart Failure Identification. *Korean Circ. J.* **2019**, *49*, 629–639. [CrossRef] [PubMed]
55. Attia, Z.I.; Kapa, S.; Yao, X.; Lopez-Jimenez, F.; Mohan, T.L.; Pellikka, P.A.; Carter, R.E.; Shah, N.D.; Friedman, P.A.; Noseworthy, P.A. Prospective validation of a deep learning electrocardiogram algorithm for the detection of left ventricular systolic dysfunction. *J. Cardiovasc. Electrophysiol.* **2019**, *30*, 668–674. [CrossRef]
56. Tripathy, R.K.; Paternina, M.R.A.; Arrieta, J.G.; Zamora-Méndez, A.; Naik, G.R. Automated detection of congestive heart failure from electrocardiogram signal using Stockwell transform and hybrid classification scheme. *Comput. Methods Prog. Biomed.* **2019**, *173*, 53–65. [CrossRef]
57. Sudarshan, V.K.; Acharya, U.R.; Oh, S.L.; Adam, M.; Tan, J.H.; Chua, C.K.; Chua, K.P.; Tan, R.S. Automated diagnosis of congestive heart failure using dual tree complex wavelet transform and statistical features extracted from 2s of ECG signals. *Comput. Biol. Med.* **2017**, *83*, 48–58. [CrossRef]
58. Wang, L.; Zhou, X. Detection of Congestive Heart Failure Based on LSTM-Based Deep Network via Short-Term RR Intervals. *Sensors (Basel)* **2019**, *19*, 1502. [CrossRef]
59. Gallagher, J.; McCormack, D.; Zhou, S.; Ryan, F.; Watson, C.; McDonald, K.; Ledwidge, M.T. A systematic review of clinical prediction rules for the diagnosis of chronic heart failure. *ESC Heart Fail.* **2019**, *6*, 499–508. [CrossRef] [PubMed]
60. Pan, W.; He, A.; Feng, K.; Li, Y.; Wu, D.; Liu, G. Multi-frequency components entropy as novel heart rate variability indices in congestive heart failure assessment. *IEEE Access.* **2019**, *7*, 37708–37717. [CrossRef]
61. Roalfe, A.K.; Mant, J.; Doust, J.A.; Barton, P.; Cowie, M.R.; Glasziou, P.; Mant, D.; McManus, R.J.; Holder, R.; Deeks, J.J.; et al. Development and initial validation of a simple clinical decision tool to predict the presence of heart failure in primary care: The MICE (male, infarction, crepitations, edema) rule. *Eur. J. Heart Fail.* **2012**, *14*, 1000–1008. [CrossRef] [PubMed]

62. Fahey, T.; Jeyaseelan, S.; McCowan, C.; Carr, E.; Goudie, B.M.; Pringle, S.D.; Donnan, P.; Sullivan, F.; Struthers, A. Diagnosis of left ventricular systolic dysfunction (LVSD): Development and validation of a clinical prediction rule in primary care. *Fam. Pract.* **2007**, *24*, 628–635. [[CrossRef](#)] [[PubMed](#)]
63. Boonman-de Winter, L.J.; Rutten, F.H.; Cramer, M.J.; Landman, M.J.; Zuithoff, N.P.; Liem, A.H.; Hoes, A.W. Efficiently screening heart failure in patients with type 2 diabetes. *Eur. J. Heart Fail.* **2015**, *17*, 187–195. [[CrossRef](#)]
64. Yamamoto, K.; Burnett, J.C., Jr.; Bermudez, E.A.; Jougasaki, M.; Bailey, K.R.; Redfield, M.M. Clinical criteria and biochemical markers for the detection of systolic dysfunction. *J. Card. Fail.* **2000**, *6*, 194–200. [[CrossRef](#)]



© 2019 by the authors. Licensee MDPI, Basel, Switzerland. This article is an open access article distributed under the terms and conditions of the Creative Commons Attribution (CC BY) license (<http://creativecommons.org/licenses/by/4.0/>).